PERGAMON

International Journal of Rock Mechanics and Mining Sciences 36 (1999) 581–596

International Journal of
Rock Mechanics
and Mining Sciences

www.elsevier.com/locate/ijrmms

Linking stress-dependent effective porosity and hydraulic conductivity fields to RMR

J. Liu[a,*], D. Elsworth[b], B.H. Brady[c]

[a]*CSIRO Division of Exploration & Mining, Private Bag, PO Wembley, WA, 6014, Australia*
[b]*Department of Energy and Geo-Environmental Engineering, The Pennsylvania State University, University Park, PA 18602, USA*
[c]*Faculty of Engineering and Mathematical Sciences, The University of Western Australia, Nedlands, Perth, WA 6907, Australia*

Accepted 13 March 1999

Abstract

Relations are developed to define changes in effective porosity and hydraulic conductivity that result from the redistribution of stresses and strains in disturbed rock masses. In each instance, changes in porosity and directional conductivities are determined from pre-disturbance porosities and conductivities, knowledge of the number of joint sets, and the indices of Rock Quality Designation (RQD) and Rock Mass Rating (RMR), defining the rock mass structure. Measured magnitudes, or estimates, of the applied strain distribution are the final required parameter. These parameters allow porosity and conductivity changes to be straightforwardly evaluated for a broad spectrum of rock mass qualities, including the representation of granular media. The model is applied to an effective stress analysis of conductivity changes that develop around a unlined circular drift in a biaxial stress field. Large increases in tangential conductivity, and reductions in radial conductivity are shown to result. These results are corroborated against the drift macropermeability test at Stripa where increases in hydraulic conductivity of the order of 1000–10000 times were measured in a 0.5–1.0 m wide zone adjacent to the excavation. © 1999 Elsevier Science Ltd. All rights reserved.

Keywords: Permeability; Porosity; Fractured media; Strains; RQD; RMR

1. Introduction

A knowledge of changes in effective porosity and hydraulic conductivity due to the redistribution of stresses or strains is crucially important in many engineering fields. Changes in effective porosity and hydraulic conductivity, as a result of thermomechanical coupling around the drifts of a radioactive waste repository, may significantly impact dryout, reflux and the transport of heat and of aqueous and colloidal contaminants [1–3]. Changes in hydraulic conductivity, induced by excavation, may induce large groundwater flows during tunnel drivage or mining, creating significant ground control problems, reducing the rate of advance [4–6], and inducing local dewatering that may affect local water supply. Underground mining changes porosity and conductivity distributions due to the redistribution of stresses. Coal seam conductivities are changed, affecting the diffusion and flow of methane, and its rate of emission to both the mine workings and to the external environment as a greenhouse gas [2,7,8]. Large strains in the overlaying strata increase permeabilities that in turn enable the dewatering of aquifers, the comingling of waters in adjacent aquifers, and in some cases the capture of streams and other surface waters [9–12]. The local ground water system may be appreciably altered in these situations [13–16], a priori prediction of these effects requiring that the controlling factors be well understood.

Rock masses have a complex internal structure and stress state, both of which are, typically, *poorly defined* and perhaps *unknowable*. This would appear to make

* Corresponding author. Tel.: +6-189-333-6169; fax: +6-189-387-8642.
E-mail address: j.liu@per.dem.csiro.au (J. Liu)

0148-9062/99/$ - see front matter © 1999 Elsevier Science Ltd. All rights reserved.
PII: S0148-9062(99)00029-7

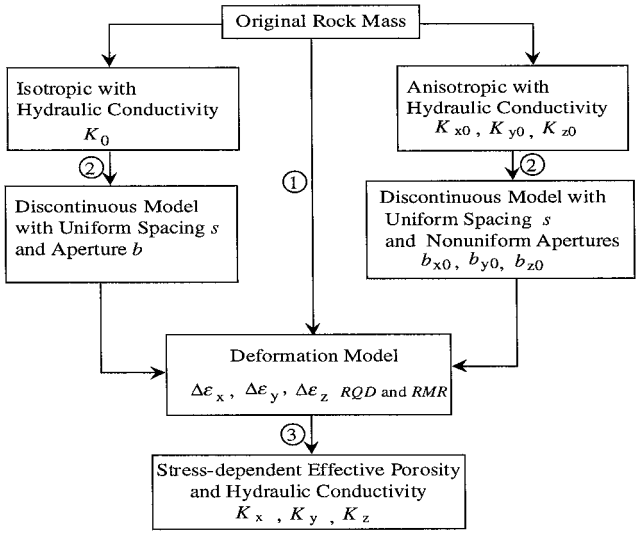

Fig. 1. Flow chart for determining the stress-dependent effective porosity and hydraulic conductivity field. Circled numbers represent steps of the analysis process. Step 1: *Deformation Analysis*. Step 2: *Hydraulic Equivalence Analysis*. Step 3: *Stress-dependent Porosity and Conductivity Analysis*.

the determination of the stress-dependent effective porosity and hydraulic conductivity field intractable. However, our understanding of the controlling processes has been improved by recent studies for both unfractured and fractured media. Microfracturing models have been used to describe the enhanced transport of methane in coal seams resulting from the development of a yield zone, using an analogy with the yielding of metal sheets [2]. These models have confirmed the presence of damage zones present around excavations in hard rocks, including those at Stripa, using simplified assumptions regarding initial fracture geometry and stress state [17,1]. Several other studies document the interaction between deformation of overlaying strata and its influence on ground water flow [18–22]. These studies have reported the effects of longwall mining on the post-mining hydraulic conductivity field and consequently on panel flow rates and the potential for dewatering. This study presents a new methodology to evaluate both stress-dependent effective porosity and stress-dependent hydraulic conductivity magnitudes from readily available rock quality indices, and for arbitrarily oriented fracture sets. The obvious advantage of the methodology is that parameters, including the initial hydraulic conductivity, the initial effective porosity, *RQD* (Rock Quality Designation) and *RMR* (Rock Mass Rating), which link the stress-dependent effective porosity and hydraulic conductivity and the induced strain, are typically available in practice. The incorporation of *RQD* and *RMR* enables the relation between effective porosity and induced strain or the relation between hydraulic conductivity and induced strain to be represented for a whole spectrum of rock masses varying from *very poor* to *very good*. Analytical solutions are developed for directional permeability changes that develop around a circular tunnel in a biaxial stress field, and corroborated against the in-situ experimental results of the drift macropermeability test at Stripa [17,1].

2. Approach

Stress- or strain-dependent porosities and hydraulic conductivities are determined from the methodology defined in Fig. 1, through the three basic steps: 1. *Deformation Analysis*. The analysis must pre-define the strain distribution, which in turn is conditioned through the constitutive relations by effective stress magnitudes. This process is necessarily iterative, since effective stresses depend on pore pressure magnitudes, which in turn depend on conductivity distributions. In some instances, however, the effects of changes in pore fluid pressures are overwhelmed by changes in total stresses, and strains may be adequately estimated without consideration of pore fluid effects. This is the case, for example in the consideration of permeability changes occasioned from longwall mining, verified in previous studies [18–20]. The evaluation of fully coupled (poroelastic) systems involving single [18] and dual [19] porosity behavior has confirmed the short-lived nature of the transient poroelastic effects. Similarly, analyses with steady-state coupling for effective stresses [20] have indicated the trivial contribution of effective stresses over the massive realignment of total stresses conditioned by mining. This assumption is not a requirement of this analysis, as strain distributions may be evaluated, inclusive of effective stress effects. However, this decoupling greatly simplifies the ensuing analysis, with little loss of applicability. 2. *Directional Hydraulic Conductivities*. It is assumed the initial hydraulic conductivity is either isotropic or anisotropic, but may be heterogeneous. The initial porous medium, with hydraulic conductivity K_0 for the isotropic case or K_{x0}, K_{y0}, and K_{z0} for the anisotropic case, is then substituted by a discontinuous model with uniform fracture spacing s and aperture b, or a discontinuous model with uniform fracture spacing s and nonuniform aperture b_{x0}, b_{y0} and b_{z0}, respectively. This substitution suggests that the effects of induced deformation on the hydraulic conductivity field can be analytically evaluated by introducing the modulus reduction ratio R_m, that may be defined through *RMR* [23,24], and *RQD* [25]. R_m is defined as the ratio of the elastic modulus of the rock mass to that of the intact rock. 3. *Strain Dependent Porosity and Conductivity Analysis*. Assuming that the rock matrix is functionally impermeable, and that the dominant fluid flow within the fractures may be defined by an equivalent parallel

plate model, enables the stress-dependent effective porosity and the stress-dependent hydraulic conductivity field to be determined if induced strains can be adequately partitioned between fracture and solid matrix. This partition is realized by the modulus reduction ratio, indexed to *RMR*. Fracture and matrix deformation are both linear, and deformations in normal closure or extension are the predominant hydraulic conductivity enhancing mode. Deformations are fully recoverable in this mode, with strains defined positive in extension. Hydraulic conductivity changes in compression are typically truncated by a lower threshold defining the limits of hydraulic conductivity reduction. Additionally, fracture spacing, s, does not change with the stress redistribution. Under these assumptions, both the stress-dependent effective porosity and the stress-dependent hydraulic conductivity field is defined as a function of the initial hydraulic conductivity K_0 for the isotropic case and K_{x0}, K_{y0}, and K_{z0} for the anisotropic case, together with *RQD, RMR*, and induced strains $\Delta\varepsilon_x$, $\Delta\varepsilon_y$, and $\Delta\varepsilon_z$. Poisson effects on hydraulic conductivity are small and are neglected in this exposition. The interested reader may confirm the magnitude of this effect from the material included in the Appendix.

3. Deformation analysis

As discussed above, it is assumed that deformations in normal closure or extension of fractures are the predominant hydraulic conductivity enhancing mode. Therefore, the induced normal strains are of interest. The induced strains, $\Delta\varepsilon_x$, $\Delta\varepsilon_y$, and $\Delta\varepsilon_z$, can be defined by the classic constitutive equations as

$$\begin{Bmatrix} \Delta\varepsilon_x \\ \Delta\varepsilon_y \\ \Delta\varepsilon_z \end{Bmatrix} = \frac{1}{R_m E}\begin{bmatrix} 1 & -\nu & -\nu \\ -\nu & 1 & -\nu \\ -\nu & -\nu & 1 \end{bmatrix}\left\{\begin{Bmatrix} \Delta\sigma_x \\ \Delta\sigma_y \\ \Delta\sigma_z \end{Bmatrix} - \alpha^* p \begin{Bmatrix} 1 \\ 1 \\ 1 \end{Bmatrix}\right\} \tag{1}$$

where E is elastic modulus of the rock matrix, ν is Poisson ratio, p is pore water pressure, α^* is a Biot constant, and $\Delta\sigma_x$, $\Delta\sigma_y$, $\Delta\sigma_z$ are components of the total normal stress in the x-, y- and z-directions, respectively, and R_m is the modulus reduction ratio. R_m is defined as the ratio of the elastic modulus of the rock mass to that of the intact rock, always less than unity [26,27]. Empirical relations exist to scale this ratio directly with rock mass classification indices [26], enabling R_m to be defined as a function of *RMR* as

$$R_m = 0.000028RMR^2 + 0.009e^{\frac{RMR}{22.82}} \tag{2}$$

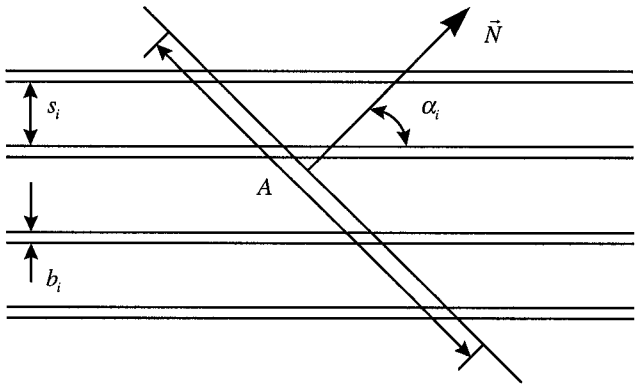

Fig. 2. Definition of directional flow in a fractured rock mass with one set of fractures, where s_i and b_i are spacing and aperture, respectively.

where *RMR* varies from 0 to 100. It is the empirical parameter, *RMR*, that determines the hydraulic response of a fractured medium to induced deformations, as presented in the following sections.

4. Directional hydraulic conductivities

A rock mass is assumed to possess n families of plane, parallel and constant width fractures with different orientations and density. As illustrated in Fig. 2, the flux, Q, across the segment can be defined [28] as

$$Q = \sum_{i=1}^{n} \frac{b_i}{s_i} AB(\mathbf{V}_i \cdot \mathbf{N}) \tag{3}$$

where b_i and s_i are fracture aperture and spacing, respectively, A is the segment length, B is the thickness (perpendicular to the section), $\mathbf{V}_i$ is the fluid velocity vector in the fractures, α_i is the angle between the direction of $\mathbf{N}$ and the strike of the fractures, and $\mathbf{N}$ is the normal vector. If the medium is continuous, the velocity, V, in the direction of $\mathbf{N}$, can be defined as

$$V = \frac{Q}{AB} \tag{4}$$

Combining Eqs. (3) and (4) gives

$$Q = \sum_{i=1}^{n} \frac{b_i}{s_i} V_i \cos\alpha_i. \tag{5}$$

If both fracture aperture and the hydraulic gradient are not large, Darcy's law is valid for both fractures and the continuous medium. Applying Darcy's law to both of them gives

$$V = -K_{\mathbf{N}} \nabla h \tag{6}$$

$$V_i = -K_i \nabla h \cos\alpha_i \tag{7}$$

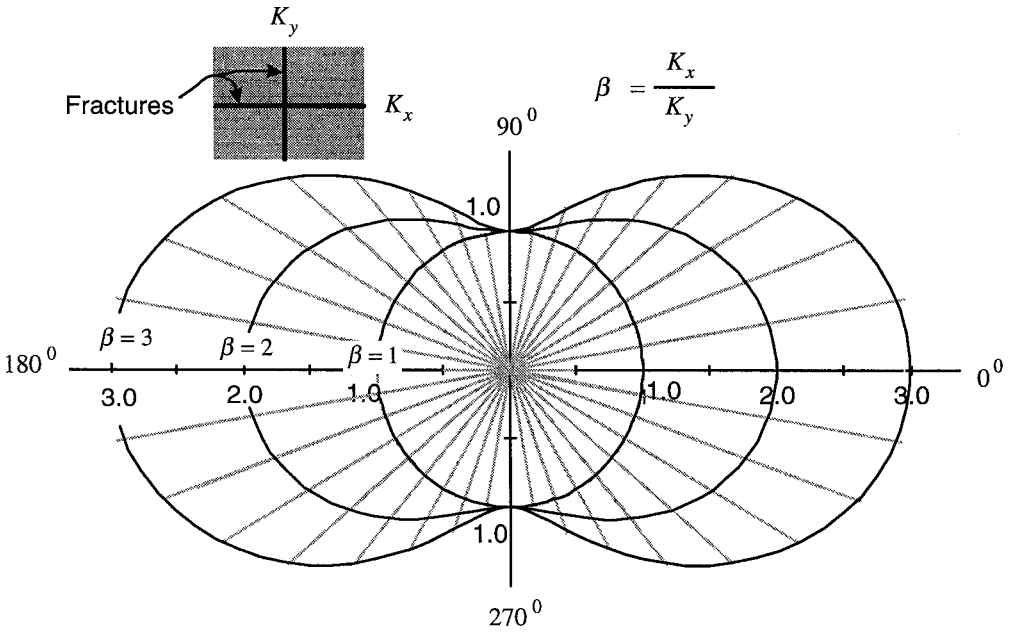

Fig. 3. Variation in hydraulic conductivity with direction of a equivalent porous medium representative of a fractured medium with two orthogonal sets of fractures under different β values.

where h is total head, and $K_{\mathbf{N}}$ and K_i are the directional **N** conductivity in the **N** direction and the conductivity in the ith set of fractures, respectively. Substituting Eq. (6) and (7) into (5) yields

$$K_{\mathbf{N}} = \sum_{i=1}^{n} \frac{b_i}{s_i} K_i \cos^2 \alpha_i. \tag{8}$$

For rock masses with either one set or two orthogonal sets of identical fractures, Eq. (8) is simplified as,

$$K_{\mathbf{N}} = \frac{b}{s} K_f \cos^2 \alpha \tag{9}$$

$$K_{\mathbf{N}} = \frac{b}{s} K_f \tag{10}$$

respectively. It is apparent that the hydraulic conductivity field of the equivalent continuous medium for a rock mass with only one set of fractures is highly anisotropic, and that the hydraulic conductivity field of

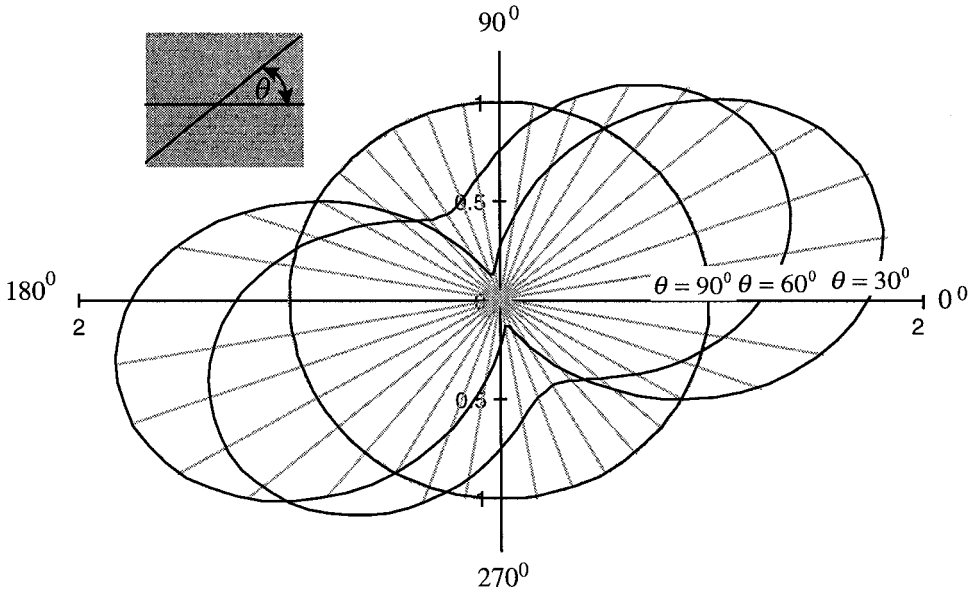

Fig. 4. Variation in hydraulic conductivity with direction of an equivalent porous medium representative of a fractured medium with two sets of fractures under different combinations.

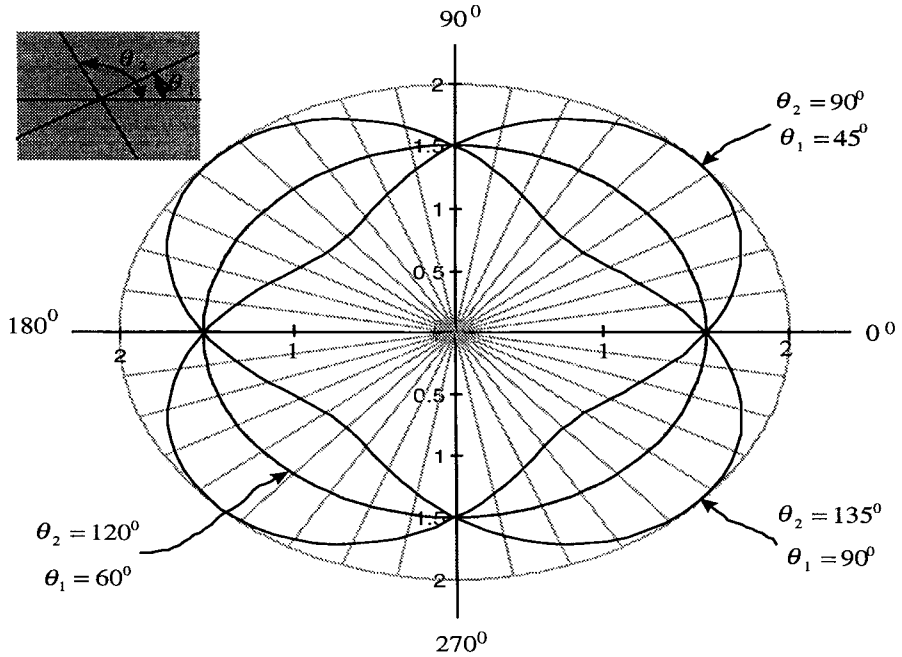

Fig. 5. Variation in hydraulic conductivity with direction of an equivalent porous medium representative of a fractured medium with three sets of fractures under different combinations.

the equivalent continuous medium for a rock mass with two orthogonal sets of identical fractures is isotropic. Therefore, the rock mass with two orthogonal sets of identical fractures can be substituted by an equivalent continuous medium. This conclusion is also demonstrated numerically [29]. For a rock mass with three orthogonal sets of identical fractures, hydraulic conductivities in the three orthogonal directions (assuming they are coincident with the three fracture orientations), K_x, K_y and K_z, can be obtained by incorporating the contribution of the third set of fractures into Eq. (10)

$$K_x = K_y = K_z = \frac{2b}{s}K_f. \tag{11}$$

Eqs. (10) and (11) imply that an isotropic medium can be substituted by a discontinuous model with two orthogonal sets of identical fractures for the two-dimensional case or with three orthogonal sets of identical fractures for the three-dimensional case, and vice versa. These conclusions are consistent with the previous results of Snow [30]. By applying Monte Carlo methods, Snow [30] concluded that two orthogonal sets with equal properties have the anisotropic permeability of a prolate spheroid, with maximum parallel to the intersection of the sets twice that on *an isotropic plane* normal to both sets, and that three equal orthogonal sets are statistically isotropic.

Eq. (8) is used to evaluate the equivalent hydraulic conductivities of both fractured and porous media. Assuming there are two sets of fractures and $\beta = \frac{K_1}{K_2}$, Eq. (8) may be rewritten as

$$\frac{K_N}{K_1} = \beta \cos^2\alpha_1 + \cos^2\alpha_2. \tag{12}$$

Eq. (12) is illustrated graphically in Figs. 3 and 4. Variation in hydraulic conductivity of the equivalent medium for a fractured medium with two orthogonal sets of fractures under different values of β ($K_1 = K_x$ and $K_2 = K_y$) is plotted with direction in Fig. 3. It is apparent that the value of β is a measure of anisotropy for the equivalent medium. If $\beta = 1$, the equivalent medium behaves isotropically. Otherwise, it behaves anisotropically. Assuming $\beta = 1$, the hydraulic anisotropy of the equivalent medium evolves with the angle, θ, between two sets of fractures, as shown in Fig. 4. The two principal directions of hydraulic conductivities are controlled by the value of θ. Furthermore, the hydraulic anisotropy of the equivalent medium is determined not only by the conductivity ratio value of β, but also by the value of θ, as demonstrated in Figs. 3 and 4. This conclusion is consistent with numerical results [29].

Assuming $\beta = 1$ and the presence of three sets of fractures, as illustrated in Fig. 5, where θ_1 and θ_2 describe the relative orientations, Eq. (8) is rewritten as

$$\frac{K_N}{K_1} = \cos^2\alpha_1 + \cos^2(\theta_1 - \alpha_1) + \cos^2(\theta_2 - \alpha_1). \tag{13}$$

Eq. (13) is shown graphically in Fig. 5. It is shown that the principal directions of hydraulic conductivity for the equivalent medium vary with the values of θ_1 and θ_2, and that the equivalent medium behaves iso-

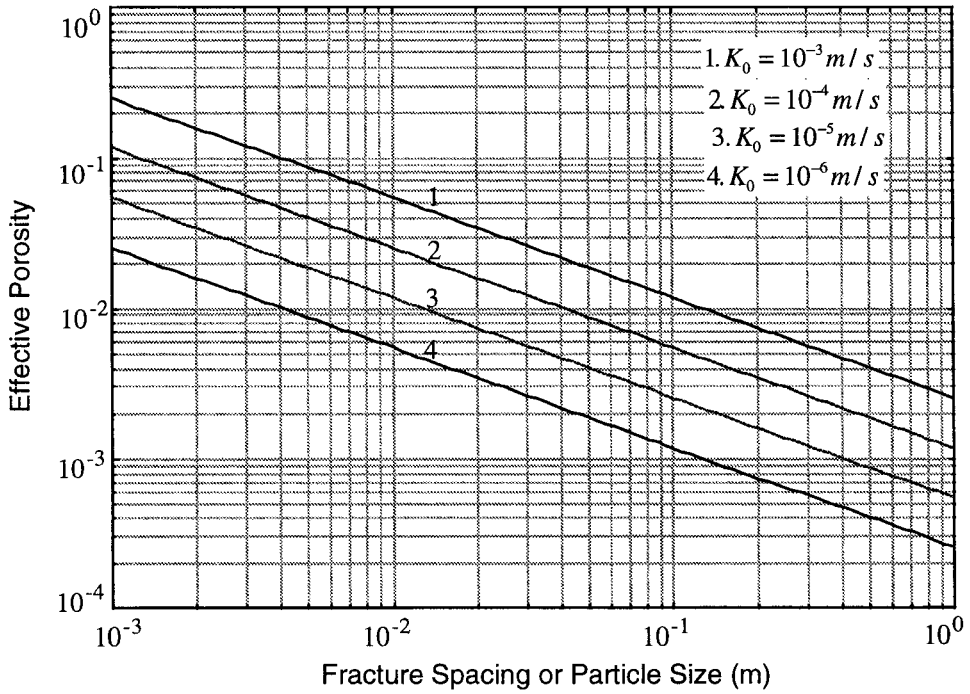

Fig. 6. Relations between fracture spacing and effective porosity under different isotropic hydraulic conductivities.

tropically only when $\theta_1 = 60^\circ$ and $\theta_2 = 120^\circ$. Otherwise, it behaves anisotropically. It can be inferred from these examples that the fractured medium behaves isotropically when the angle between two adjacent sets of fractures satisfies

$$\theta = \frac{360^\circ}{2n} \tag{14}$$

where n is the number of fracture sets; for example, $\theta = 90^\circ$ when $n = 2$; $\theta = 60^\circ$ when $n = 3$, and $\theta = 45^\circ$ when $n = 4$. These results provide the basis for the equivalence between fractured and porous media under certain conditions.

5. Hydraulic conductivity–effective porosity relations

If it is assumed that the in-situ hydraulic conductivity is equal to K_0, substituting $K_N = K_0$ and $K_f = \frac{gb^2}{12\mu}$ [31] into Eqs. (10) and (11), the equivalent fracture aperture for the two-dimensional and three-dimensional cases are defined as

$$b = \left(\frac{12\mu s K_0}{g}\right)^{\frac{1}{3}} \tag{15}$$

$$b = \left(\frac{6\mu s K_0}{g}\right)^{\frac{1}{3}} \tag{16}$$

respectively, where μ is kinematic viscosity, and g is gravitational acceleration. Consequently, the effective porosity for both the two-dimensional case and the three-dimensional case are defined as

$$\phi_f^0 = \frac{(b+s)^3 - s^2}{(b+s)^2} \cong \frac{2b}{s} = 2\left(\frac{12\mu K_0}{g s^2}\right)^{\frac{1}{3}} \tag{17}$$

$$\phi_f^0 = \frac{(b+s)^3 - s^3}{(b+s)^3} \cong \frac{3b}{s} = 3\left(\frac{6\mu K_0}{g s^2}\right)^{\frac{1}{3}} \tag{18}$$

respectively.

The relation between effective porosity and fracture spacing, as shown in Eq. (18), is illustrated graphically in Fig. 6. Eq. (18) may be interpreted as a microscale model, assuming the material is made of cubes and s is the side dimension of the cube. When s is small, it represents a medium made of very fine grains. In other words, it represents granular soil. When s is large, it represents a medium made of large "grains" or rock blocks. As illustrated in Fig. 6, the effective porosity decreases as the value of s increases for a constant magnitude of hydraulic conductivity, K_0. This is typically observed where soils have much higher effective porosities than rock masses. Eq. (18) is an unified expression of the effective porosity for isotropic soils and rock masses.

As shown in Eq. (18), the effective porosity of rock masses is a function of hydraulic conductivity, K_0, and the equivalent fracture spacing, s. The hydraulic conductivity can be determined by in-situ hydraulic tests.

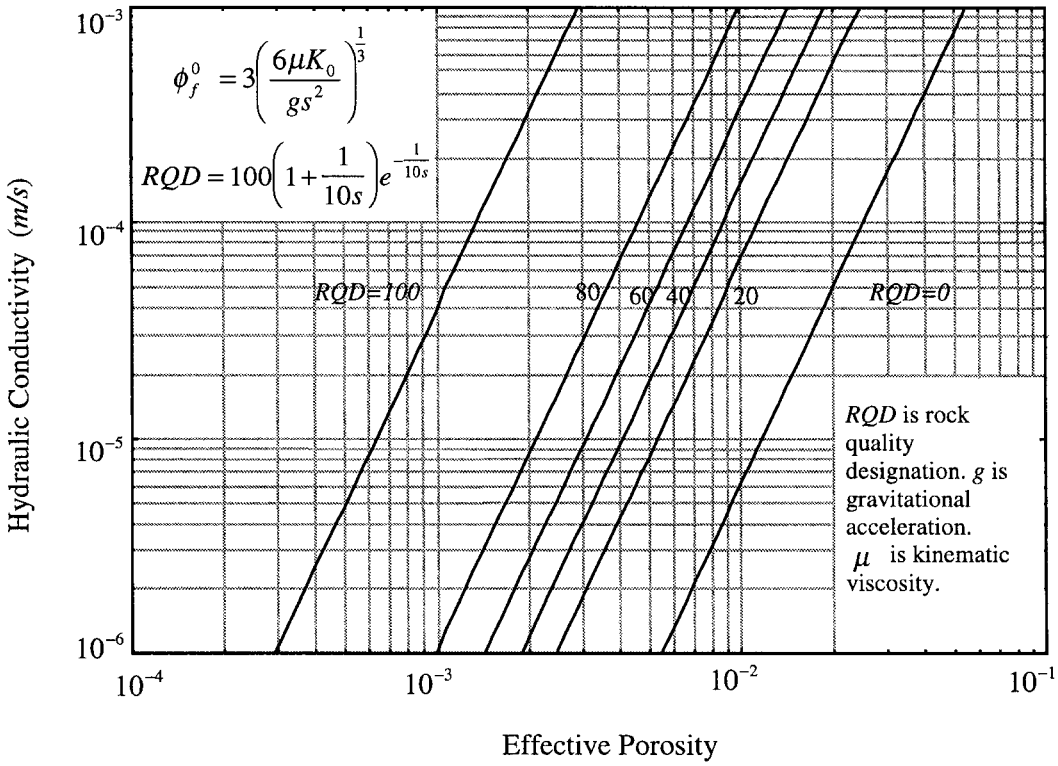

Fig. 7. Relation between hydraulic conductivity, K_0, and effective porosity, ϕ_f^0, under different values of *RQD*.

The equivalent fracture spacing is determined by an empirical rock classification index, *RQD* (Rock Quality Designation), defined as [25]

$$RQD = 100\sum_{i=1}^{n}\frac{X_i}{L} \tag{19}$$

where n is the number of intact lengths greater than 10 cm, L is the length of a drill hole or scanline, and X_i is the intact length. Assuming that the fractures occur randomly, the resulting Poisson process defines the intact lengths to have a negative exponential distribution, Priest and Hudson [32] derived the following relation

$$RQD = 100(1+0.1\lambda)\mathrm{e}^{-0.1\lambda} \tag{20}$$

where λ is the average number of fractures per meter. Substituting $s=\frac{1}{\lambda}$ into Eq. (20) gives

$$RQD = 100\left(1+\frac{1}{10s}\right)\mathrm{e}^{-\frac{1}{10s}} \tag{21}$$

where s is the equivalent fracture spacing. The effective porosity can be obtained from Fig. 7 if the hydraulic conductivity and the value of *RQD* for a specific rock mass are known. The incorporation of *RQD* into the determination of effective porosity makes it possible to link the effective porosity to an empirical geotechnical parameter which is easily available in practice. When *RQD* approaches zero, the rock mass is highly fractured and may be represented as a granular medium with a relatively high effective porosity. Behavior is bounded in the range $0 < RQD < 100$, enabling changes in porosity and conductivity to be determined for a full range of fractured and granular media.

6. Strain-dependent conductivity–porosity relations

As discussed above, an isotropic medium can be substituted by a fractured medium with two orthogonal sets of identical fractures for the two-dimensional case, and with three orthogonal sets of identical fractures for the three-dimensional case. Similarly, an anisotropic medium can be approximately substituted by a fractured medium with one set of fractures for the one-dimensional case, two orthogonal sets of non-identical fractures for the two-dimensional case, and with three orthogonal sets of non-identical fractures for the three-dimensional case. These substitutions enable both the hydraulic conductivity to be defined as a function of *RQD* and fracture spacing (grain size for soil) for natural soils and rock masses, and the hydraulic conductivity to be defined as a function of induced strains, *RMR*, and *RQD* for the modified soils and rock masses. Based on the substituted fracture models, the following relations between fracture parameters (spacing, s, and aperture, b_{i0}, $i=x, y, z$) and hydraulic

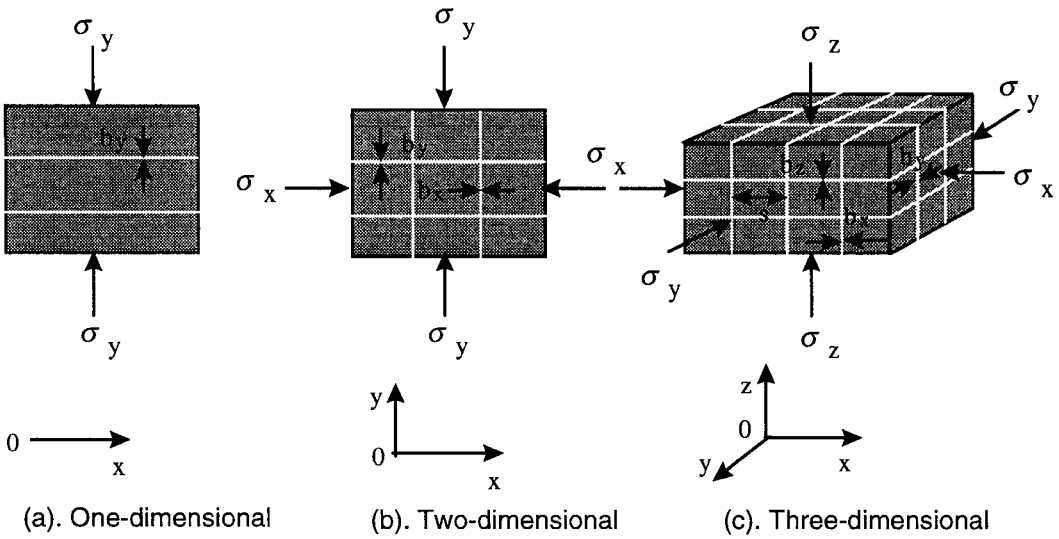

Fig. 8. Equivalent discrete hydromechanical models for the original porous medium.

conductivities (K_{x0}, K_{y0}, and K_{z0}) are obtained. For the one-dimensional case with one set of fractures, the hydraulic conductivity and the equivalent fracture aperture are defined as

$$K_{x0} = \frac{g b_{y0}^3}{12\mu s} \tag{22}$$

$$b_{y0} = \left(\frac{12\mu K_{x0} s}{g}\right)^{\frac{1}{3}} \tag{23}$$

respectively. For the two-dimensional case with two orthogonal sets of fractures, the hydraulic conductivities and equivalent fracture apertures in the x- and y-directions are defined as

$$K_{x0} = \frac{g b_{y0}^3}{12\mu s} \tag{24}$$

$$K_{y0} = \frac{g b_{x0}^3}{12\mu s} \tag{25}$$

and

$$b_{x0} = \left(\frac{12\mu K_{y0} s}{g}\right)^{\frac{1}{3}} \tag{26}$$

$$b_{y0} = \left(\frac{12\mu K_{x0} s}{g}\right)^{\frac{1}{3}} \tag{27}$$

respectively. For the three-dimensional case with three orthogonal sets of fractures, the hydraulic conductivities and the equivalent fracture apertures in the x-, y- and z-directions are defined as

$$K_{x0} = \frac{g b_{y0}^3}{12\mu s} + \frac{g b_{z0}^3}{12\mu s} \tag{28}$$

Table 1
Relations between parameters

Dimensionality	3D	2D	1D
Spacing	s	s	s
Initial aperture	$b_{x0}\ b_{y0}\ b_{z0}$	$b_{x0}\ b_{y0}$	b_{y0}
Change in aperture	$s(1-R_m)\Delta\varepsilon_x$ $s(1-R_m)\Delta\varepsilon_y$ $s(1-R_m)\Delta\varepsilon_z$	$s(1-R_m)\Delta\varepsilon_x$ $s(1-R_m)\Delta\varepsilon_y$	$s(1-R_m)\Delta\varepsilon_y$
Initial areal porosity	$\phi_f^{x0} = \frac{b_{y0}+b_{z0}}{s}$ $\phi_f^{y0} = \frac{b_{x0}+b_{z0}}{s}$ $\phi_f^{z0} = \frac{b_{x0}+b_{y0}}{s}$	$\phi_f^{x0} = \frac{b_{y0}}{s}$ $\phi_f^{y0} = \frac{b_{x0}}{s}$	$\phi_f^{x0} = \frac{b_{y0}}{s}$
Initial volumetric porosity	$\phi_f^0 = \frac{b_{x0}+b_{y0}+b_{z0}}{s}$	$\phi_f^0 = \frac{b_{x0}+b_{y0}}{s}$	$\phi_f^0 = \frac{b_{y0}}{s}$
Changed areal porosity	$\phi_f^x = \phi_f^{x0} + (1-R_m)(\Delta\varepsilon_y + \Delta\varepsilon_z)$ $\phi_f^y = \phi_f^{y0} + (1-R_m)(\Delta\varepsilon_x + \Delta\varepsilon_z)$ $\phi_f^z = \phi_f^{z0} + (1-R_m)(\Delta\varepsilon_x + \Delta\varepsilon_y$	$\phi_f^x = \phi_f^{x0} + (1-R_m)\Delta\varepsilon_y$ $\phi_f^y = \phi_f^{y0} + (1-R_m)\Delta\varepsilon_x$	$\phi_f^x = \phi_f^{x0} + (1\text{-}R_m)\Delta\varepsilon_y$
Changed volumetric porosity	$\phi_f = \phi_f^0 + (1-R_m)\Delta\varepsilon_v$ $\Delta\varepsilon_v = \Delta\varepsilon_x + \Delta\varepsilon_y + \Delta\varepsilon_z$	$\phi_f = \phi_f^0 +$ $(1-R_m)(\Delta\varepsilon_x + \Delta\varepsilon_y)$	$\phi_f = \phi_f^0 + (1-R_m)\Delta\varepsilon_y$

$$K_{y0} = \frac{gb_{x0}^3}{12\mu s} + \frac{gb_{z0}^3}{12\mu s} \tag{29}$$

$$K_{z0} = \frac{gb_{x0}^3}{12\mu s} + \frac{gb_{y0}^3}{12\mu s} \tag{30}$$

and

$$b_{x0} = \left[\frac{6\mu s}{g}(K_{y0} + K_{z0} - K_{x0})\right]^{\frac{1}{3}} \tag{31}$$

$$b_{y0} = \left[\frac{6\mu s}{g}(K_{x0} + K_{z0} - K_{y0})\right]^{\frac{1}{3}} \tag{32}$$

$$b_{z0} = \left[\frac{6\mu s}{g}(K_{x0} + K_{y0} - K_{z0})\right]^{\frac{1}{3}} \tag{33}$$

respectively. Where K_{x0}, K_{y0}, and K_{z0} are initial hydraulic conductivities in the x-, y- and z-directions, respectively, and b_{x0}, b_{y0}, and b_{z0} are equivalent apertures of the discrete model.

Fracture apertures may be changed due to the redistribution of stresses. As illustrated in Fig. 8, changes in the fracture aperture, Δb_x, Δb_y and Δb_z due to applied stresses, are determined by induced strains and fracture parameters. Relations among different parameters, defined based on Fig. 8, are documented in Table 1. Based on Table 1, stress dependent hydraulic conductivities, K_x, K_y, and K_z, are defined as

$$K_x = K_{x0}\left[1 + \frac{s(1-R_m)}{b_{y0}}\Delta\varepsilon_y\right]^3 = K_{x0}\left(\frac{\phi_f^x}{\phi_f^{x0}}\right)^3 \tag{34}$$

for the one-dimensional case with one set of fractures, as shown in Fig. 8a,

$$K_x = K_{x0}\left[1 + \frac{s(1-R_m)}{b_{y0}}\Delta\varepsilon_y\right]^3 = K_{x0}\left(\frac{\phi_f^x}{\phi_f^{x0}}\right)^3 \tag{35}$$

$$K_y = K_{y0}\left[1 + \frac{s(1-R_m)}{b_{x0}}\Delta\varepsilon_x\right]^3 = K_{y0}\left(\frac{\phi_f^y}{\phi_f^{y0}}\right)^3 \tag{36}$$

for the two-dimensional case with two orthogonal sets of fractures, as shown in Fig. 8b and

$$K_x = \frac{K_{x0}}{2}\left[1 + \frac{s(1-R_m)}{b_{y0}}\Delta\varepsilon_y\right]^3 + \frac{K_{x0}}{2}\left[1 + \frac{s(1-R_m)}{b_{z0}}\Delta\varepsilon_z\right]^3 = \frac{K_{x0}}{2}\left(\frac{\phi_f - \phi_f^y}{\phi_f^0 - \phi_{y0}}\right)^3 + \frac{K_{x0}}{2}\left(\frac{\phi_f - \phi_f^z}{\phi_f^0 - \phi_{z0}}\right)^3 \tag{37}$$

$$K_y = \frac{K_{y0}}{2}\left[1 + \frac{s(1-R_m)}{b_{x0}}\Delta\varepsilon_x\right]^3 + \frac{K_{y0}}{2}\left[1 + \frac{s(1-R_m)}{b_{z0}}\Delta\varepsilon_z\right]^3 = \frac{K_{y0}}{2}\left(\frac{\phi_f - \phi_f^x}{\phi_f^0 - \phi_{x0}}\right)^3 + \frac{K_{y0}}{2}\left(\frac{\phi_f - \phi_f^z}{\phi_f^0 - \phi_{z0}}\right)^3 \tag{38}$$

$$K_z = \frac{K_{z0}}{2}\left[1 + \frac{s(1-R_m)}{b_{x0}}\Delta\varepsilon_x\right]^3 + \frac{K_{z0}}{2}\left[1 + \frac{s(1-R_m)}{b_{y0}}\Delta\varepsilon_y\right]^3 = \frac{K_{z0}}{2}\left(\frac{\phi_f - \phi_f^x}{\phi_f^0 - \phi_{x0}}\right)^3 + \frac{K_{z0}}{2}\left(\frac{\phi_f - \phi_f^y}{\phi_f^0 - \phi_{y0}}\right)^3 \tag{39}$$

for the three-dimensional case with three orthogonal sets of fractures, as shown in Fig. 8c. Substituting $b_{x0} = b_{y0} = b_{z0} = b$ and $K_{x0} = K_{y0} = K_{z0} = K_0$ into Eqs. (34)–(39) give

$$K_x = K_0\left(1 + \frac{(1-R_m)}{\phi_f^0}\Delta\varepsilon_y\right)^3 \tag{40}$$

for the one-dimensional case with one set of fractures, as shown in Fig. 8a,

$$K_x = K_0\left[1 + \frac{2(1-R_m)}{\phi_f^0}\Delta\varepsilon_y\right]^3 \tag{41}$$

$$K_y = K_0\left[1 + \frac{2(1-R_m)}{\phi_f^0}\Delta\varepsilon_x\right]^3 \tag{42}$$

for the two-dimensional case with two orthogonal sets of fractures, as shown in Fig. 8b and

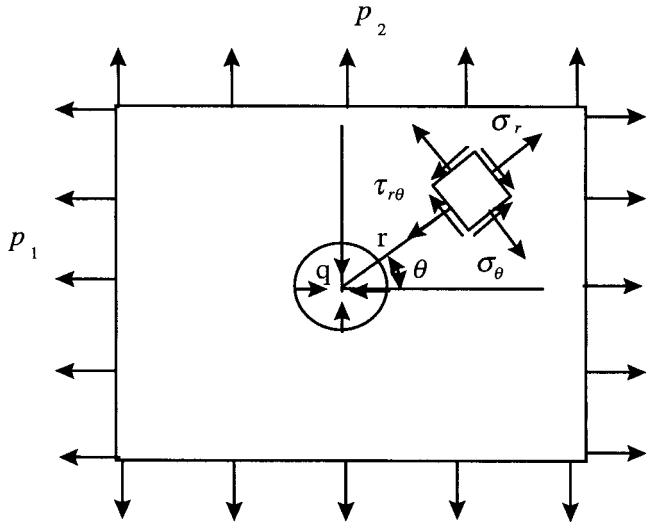

Fig. 9. Simplified representation for a circular excavation made within a biaxial stressed medium. The far stress field biaxial stresses are equal to p_1 and p_2, respectively. q is the fluid pressure in the circular opening.

$$K_x = \frac{K_0}{2}\left[1 + \frac{3(1-R_m)}{\phi_f^0}\Delta\varepsilon_y\right]^3 + \frac{K_0}{2}\left[1 + \frac{3(1-R_m)}{\phi_f^0}\Delta\varepsilon_z\right]^3 \quad (43)$$

$$K_y = \frac{K_0}{2}\left[1 + \frac{3(1-R_m)}{\phi_f^0}\Delta\varepsilon_x\right]^3 + \frac{K_0}{2}\left[1 + \frac{3(1-R_m)}{\phi_f^0}\Delta\varepsilon_z\right]^3 \quad (44)$$

$$K_z = \frac{K_0}{2}\left[1 + \frac{3(1-R_m)}{\phi_f^0}\Delta\varepsilon_x\right]^3 + \frac{K_0}{2}\left[1 + \frac{3(1-R_m)}{\phi_f^0}\Delta\varepsilon_y\right]^3 \quad (45)$$

for the three-dimensional case with three orthogonal sets of fractures, as shown in Fig. 8c. As shown in Eqs. (40)–(45), the stress dependent hydraulic conductivities are uniquely defined by the original hydraulic conductivity, K_0, $R_m(RMR)$, ϕ_f^0 $(K_0;\ RQD)$, and induced strains. The most obvious advantage of these relations is that these parameters are readily available in practice.

7. Circular tunnel in a biaxial stress field

The method developed in the previous is applied to a circular tunnel (Fig. 9) within a biaxial stress field, p_1 and p_2, also representing the geometry of a well or borehole present within a fractured medium. Fluid is injected at pressure q at the borehole wall.

Assuming elastic behavior [33], excavation-induced strains are defined as

$$\Delta\varepsilon_r = \frac{1-\nu^2}{E}\left[\frac{3(p_1-p_2)a^4\cos 2\theta}{2(1-\nu)r^4} - \frac{(p_1+p_2)a^2}{2(1-\nu)r^2} - \frac{2(p_1-p_2)a^2\cos 2\theta}{r^2}\right] + \frac{(1+\nu)a^2}{Er^2}q \quad (46)$$

$$\Delta\varepsilon_\theta = \frac{1-\nu^2}{E}\left[\frac{3(p_1-p_2)a^4\cos 2\theta}{2(1-\nu)r^4} + \frac{(p_1+p_2)a^2}{2(1-\nu)r^2} + \frac{4\nu(p_1-p_2)a^2\cos 2\theta}{(1-\nu)r^2}\right] - \frac{(1+\nu)a^2}{Er^2}q \quad (47)$$

where $\Delta\varepsilon_r$ and $\Delta\varepsilon\theta$ are components of the induced strain in the radial (r-) and tangential (θ-) directions, respectively; E is the elastic modulus of rock mass, ν is the Poisson ratio, and a is the radius of the opening. Substituting Eqs. (46) and (47) into (35) and (36), hydraulic conductivity ratios are defined as

$$\frac{K_r}{K_0} = \left\{1 + \beta\frac{1-\nu^2}{E}\left[-\frac{3(p_1-p_2)a^4\cos 2\theta}{2(1-\nu)r^4} + \frac{(p_1+p_2)a^2}{2(1-\nu)r^2} + \frac{4\nu(p_1-p_2)a^2\cos 2\theta}{(1-\nu)r^2}\right] - \beta\frac{(1+\nu)a^2}{Er^2}q\right\}^3 \quad (48)$$

$$\frac{K_\theta}{K_0} = \left\{1 + \beta\frac{1-\nu^2}{E}\left[\frac{3(p_1-p_2)a^4\cos 2\theta}{2(1-\nu)r^4} - \frac{(p_1+p_2)a^2}{2(1-\nu)r^2} - \frac{2(p_1-p_2)a^2\cos 2\theta}{r^2}\right] + \beta\frac{(1+\nu)a^2}{Er^2}q\right\}^3 \quad (49)$$

where the parameter, β, is defined as

$$\beta = \frac{2(1-R_m)}{\phi_f^0} \quad (50)$$

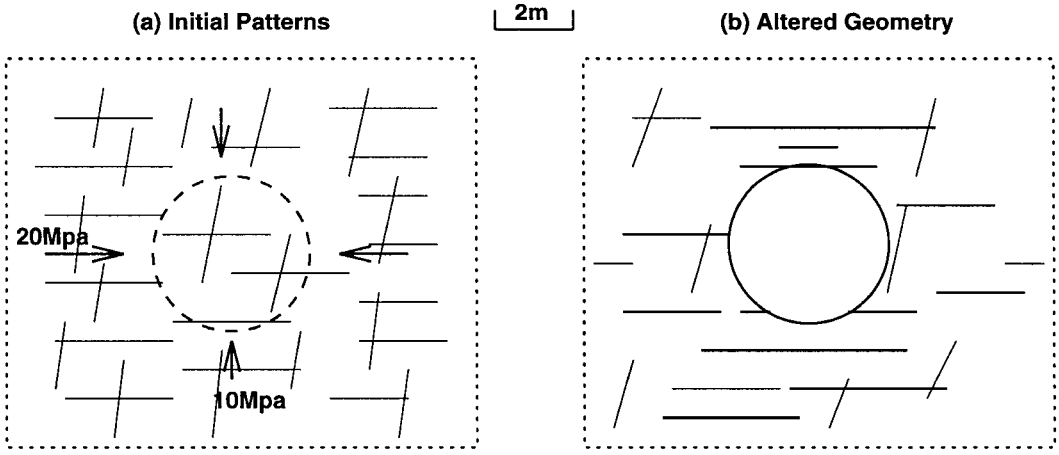

Fig. 10. Hypothetical stress-induced alteration of granitic fracture geometry. Notice expansion and generation of subhorizontal fractures and closure of steeply oriented fractures at crown and floor.

where the effective porosity, $\phi^0{}_f$, and the modulus reduction factor, R_m, are defined by Eqs. (18) and (2), respectively. Eqs. (48) and (49) are rewritten as

$$\frac{K_r}{K_0} = \left\{1 + \beta\varepsilon^p\left[-\frac{3(\alpha-1)a^4\cos 2\theta}{2r^4} + \frac{(\alpha+1)a^2}{2r^2} + \frac{4\nu(\alpha-1)a^2\cos 2\theta}{r^2}\right] - \beta\varepsilon^q\frac{a^2}{r^2}\right\}^3 \quad (51)$$

$$\frac{K_\theta}{K_0} = \left\{1 + \beta\varepsilon^p\left[+\frac{3(\alpha-1)a^4\cos 2\theta}{2r^4} - \frac{(\alpha+1)a^2}{2r^2} - \frac{2(\alpha-1)(1-\nu)a^2\cos 2\theta}{r^2}\right] + \beta\varepsilon^q\frac{a^2}{r^2}\right\}^3 \quad (52)$$

where α, ε^p and ε^q are defined as

$$\alpha = \frac{p_1}{p_2} \quad (53)$$

$$\varepsilon^p = \frac{(1+\nu)p_2}{E} \quad (54)$$

$$\varepsilon^q = \frac{(1+\nu)q}{E} \quad (55)$$

respectively. As shown in Eqs. (51) and (52), the magnitudes of change in hydraulic conductivities are regulated by the parameter, β, which is a function of the *RQD* and the *RMR*. These two parameters are readily available in practice. For a particular rock mass, the magnitudes of change in hydraulic conductivities are regulated by strains on the excavation surface, ε^p and ε^q, which are a function of external loads and the elastic modulus of the rock mass.

The Buffer Mass Test was conducted in the Stripa mine over the period 1981–1985 [1,17]. This test was designed to measure the permeability of a large volume of low permeability fractured rock by monitoring water flow into a 33 m long section of a tunnel. The radius of the tunnel is about 2.5 m with two major sets of fractures striking obliquely to the tunnel axis, as illustrated in Fig. 10a. Fracture frequency measured in holes drilled from the tunnel was on average 4.5 joints/m in inclined holes and 2.9 joints/m in vertical holes [17]. The initial stress field is anisotropic with a high horizontal stress component and the conductivity of the virgin rock is about 10^{-10} m/s. The excavation of the test drift produced a dramatic increase in axial hydraulic conductivity in a narrow zone adjacent to the periphery of the drift. The conductivity increase is estimated to be of the order of 1000 times. It is observed that the piezometric head is 40–90 m of water at about a 2 m distance from the periphery of the drift and 80–130 m at 10 m distance. The hydraulic gradient is approximately 5. It was concluded from the pressure gradient that a "skin" of lower radial permeability surrounds the drift. This skin effect determines that water flowing towards the drift may be effectively discharged through the rock in the axial direction of the drift. It is believed [1] that there are considerable effects of the excavation-induced stress changes on the water-bearing capacity of pre-existing fractures which will be widened, compressed, extended or shortened depending on their orientation as well as on the prevailing stress field, as illustrated in Fig. 10b.

Assuming that: (1) A statistically uniform aperture and spacing distribution exists prior to excavation; (2) Fracture spacing and continuity are not altered by the excavation; (3) Stress changes may be adequately calculated by elastic theory; and (4) Water-bearing capacity of individual fractures are determined by the normal stress; the stress-dependent hydraulic conductivity field is evaluated by the method developed in this study. The experimental hydraulic conductivity for

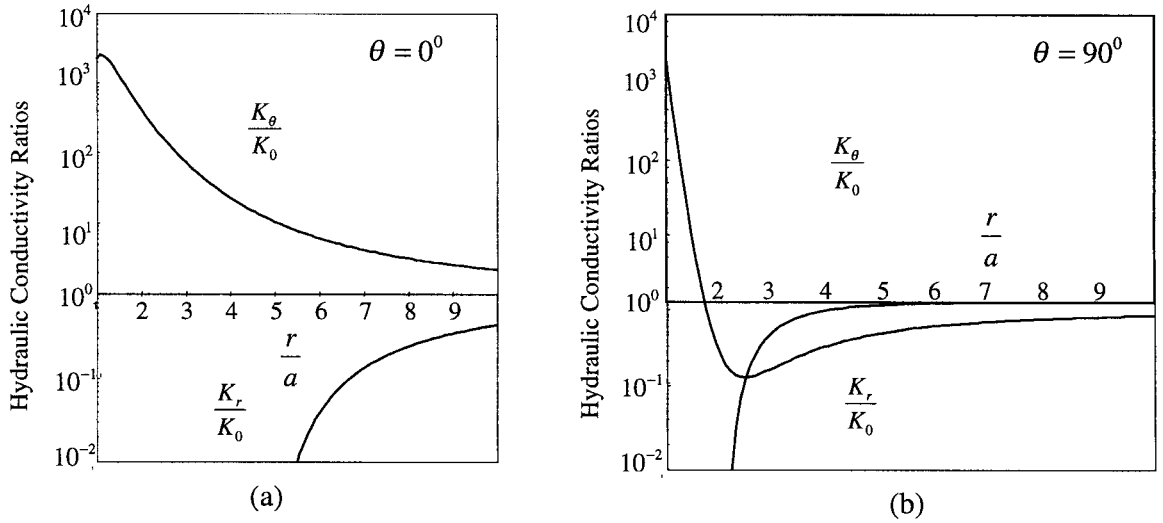

Fig. 11. Distribution of hydraulic conductivity ratios around a circular underground excavation present in a biaxial stressed medium ($p_1 = 20$ MPa, $p_2 = 10$ MPa). Where α is the radius of the excavation and r is the distance away from the excavation center. $\theta = 0^\circ$ represents the horizontal direction and $\theta = 90^\circ$ the vertical direction.

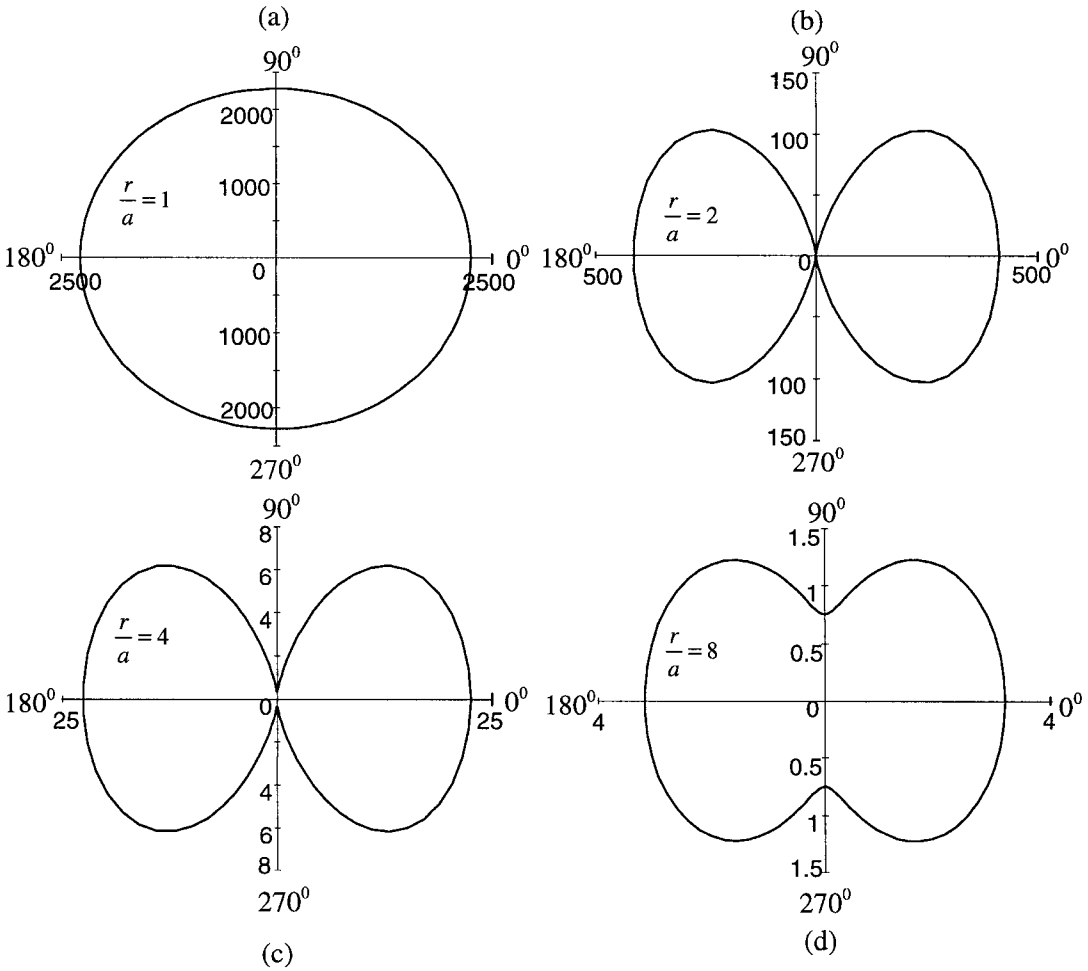

Fig. 12. Variation in hydraulic conductivity ratios of $\frac{K_\theta}{K_0}$ with direction. Where a is the radius of a underground circular excavation, made in a biaxial stressed medium ($p_1 = 20$ MPa, $p_2 = 10$ MPa), and r is the distance away from the excavation center.

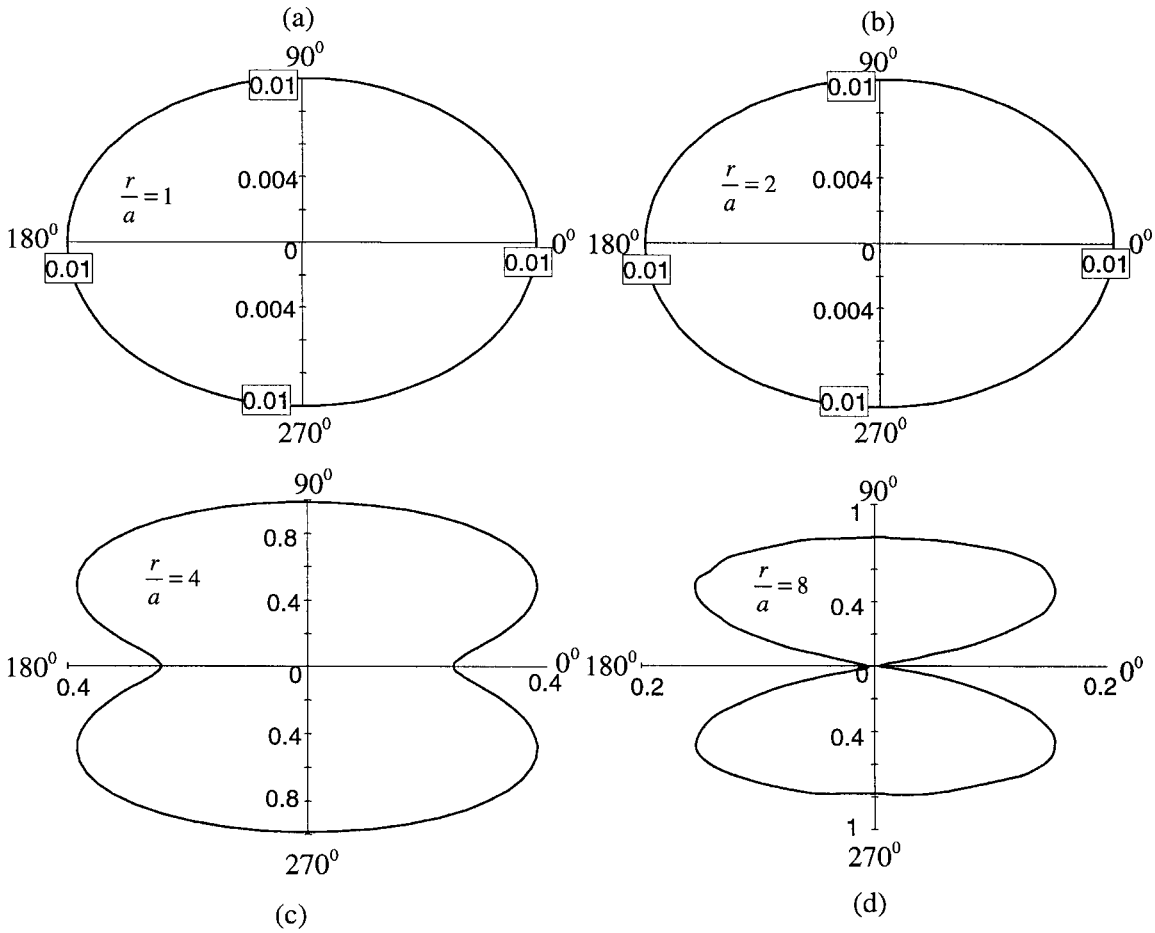

Fig. 13. Variation in hydraulic conductivity ratios of $\frac{K_r}{K_0}$ with direction. Where a is the radius of a underground circular excavation, made in a biaxial stressed medium ($p_1 = 20$ MPa, $p_2 = 10$ MPa), and r is the distance away from the excavation center.

the virgin rock is taken as $K_0 = 10^{-10}$ m/s. The observed fracture spacings are averaged as $s = 0.27$ m. The far field stress is taken as $p_1 = 20$ MPa, and $p_2 = 10$ MPa. The elastic modulus and Poisson ratio are assumed as 37.5 GPa and 0.25, respectively. The value of *RMR* is taken as 70. Substituting these numbers into Eqs. (51) and (52) yields

$$\frac{K_r}{K_0} = \left(1 + 18.225\frac{a^4}{r^4} \cos 2\theta - \frac{12.15a^2}{r^2} - \frac{12.15a^2 \cos 2\theta}{r^2}\right)^3 \quad (56)$$

$$\frac{K_\theta}{K_0} = \left(1 - 18.225\frac{a^4}{r^4} \cos 2\theta + \frac{12.15a^2}{r^2} + \frac{18.225a^2 \cos 2\theta}{r^2}\right)^3. \quad (57)$$

Eqs. (56) and (57) are graphically shown in Figs. 11–13. Assuming $\theta = 0°$ and $\theta = 90°$, the distribution of hydraulic conductivity ratios around the circular tunnel is shown in Fig. 11. It is apparent that the these theoretical results are consistent with the experimental results reported for the *buffer mass* test at Stripa. Furthermore, the approximate variation in hydraulic conductivity ratios of $\frac{K_\theta}{K_0}$ and $\frac{K_r}{K_0}$ with direction are plotted in Figs. 12 and 13, respectively. The results are exact on the horizontal and vertical axes, but for intermediate orientations are approximate, due to the assumption of radial and tangential fractures. Changes in tangential and radial hydraulic conductivities are more pronounced at springline, than at crown or invert. Tangential conductivities are greatly increased as changes in strain (or stress) cause the changes in conductivity. Radial conductivities are greatly diminished, as a result of closure on radial (horizontal) fractures. These effects diminish to background levels by about ten tunnel radii. Conductivity changes are less pronounced in the crown as the change in vertical stress is relatively smaller than at springline. Of interest is the accentuation in permeability anisotropy that results, with high tangential permeabilities and low radial permeabilities. These distributions would not automatically result in large drift inflows, unless the

compressional skin at the tunnel wall is breached; a situation that is quite likely in practice.

8. Conclusions

Changes in the effective porosity and hydraulic conductivity fields, due to the redistribution of stresses, can be predicted by the methodology developed in this study. The clear advantage of the methodology is that parameters, including the initial hydraulic conductivity, *RQD*, and *RMR*, which link the stress-dependent hydraulic conductivity and effective porosity and the excavation-induced strain, are readily available in practice. The incorporation of *RMR* enables the relation between effective porosity and induced strain or the relation between hydraulic conductivity and induced strain to represent a broad spectrum of rock masses from very poor to very good. When $RMR = 100$, the laboratory modulus can be used to directly represent rock mass without any reduction. This results in the smallest change in both hydraulic conductivity and effective porosity because the induced strain is uniformly distributed between fractures and matrix. When *RMR* approaches zero, the laboratory modulus must be reduced at least 100 times in order to accurately represent the response of the rock mass. This results in the largest possible change in both hydraulic conductivity and effective porosity because the induced strain is applied entirely to the fracture system. These values of *RMR* bound the possible ranges in behavior of the system in a natural and mechanically defensible manner.

These relationships may be readily applied to the practical evaluation of permeability changes in disturbed rock masses. As an example, a solution is developed for a tunnel within a biaxial stress field, to validate the methodology against the in-situ experimental results of the drift macropermeability test at Stripa. The results define modes and magnitudes of permeability enhancement, resulting in an axial rind of high tangential conductivities around the excavation that reach as far as ten radii from the drift wall. Compressive hoop stresses reduce radial permeabilities at the drift, but will be breached as higher field stress obliquities result. For uniaxial field stresses, extensional hoop stresses result over a portion of the drift periphery, that in turn will develop increased conductivities.

Acknowledgements

The work reported in this paper was supported by the National Science Foundation under Grant No. MSS-9209059 and by the Australian Research Council under Large Grant No. A89600730. The sources of this support are gratefully acknowledged. The authors also thank two anonymous reviewers for providing critical comments and constructive suggestions in revising the manuscript.

Appendix A. Poisson effect on conductivity change

Where the strains resulting from Poisson expansion are incorporated in the analysis, strains applied in any of the principal directions, will result in conductivity changes of fracture sets aligned parallel with that direction. This will result in off diagonal terms in the conductivity change tensor, even if the original conductivities are principal conductivities and the off-diagonal terms are therefore null. Changes in conductivity may be evaluated, in generality, from $K = K_0 = (1 + \frac{\Delta b}{b_0})^3$. To simplify the analysis, three sets of orthogonal fractures are considered, each of equal spacing, s, initial aperture, b_0, and equivalent stiffness characteristics. Changes in aperture are defined relative to the fracture plane orthogonal to the direction of the coordinate axis under consideration. The aperchange relationships, inclusive of the off-diagonal components, may be defined as:

$$\begin{Bmatrix} \Delta b_x/b_0 \\ \Delta b_y/b_0 \\ \Delta b_z/b_0 \end{Bmatrix} = \begin{bmatrix} [(1-R_m)\frac{s}{b_0} + 1 - A] & R_m H \frac{s}{b_0} & R_m H \frac{s}{b_0} \\ R_m H \frac{s}{b_0} & [(1-R_m)\frac{s}{b_0} + 1 - A] & R_m H \frac{s}{b_0} \\ R_m H \frac{s}{b_0} & R_m H \frac{s}{b_0} & [(1-R_m)\frac{s}{b_0} + 1 - A] \end{bmatrix} \begin{Bmatrix} \Delta \varepsilon_x \\ \Delta \varepsilon_y \\ \Delta \varepsilon_z \end{Bmatrix} \quad (58)$$

where R_m is the modulus reduction ratio, defined previously, ν is the Poisson ratio of the matrix, and $A = 2\nu R_m H$ with $H = \nu/(\frac{1}{R_m} - \nu)$. The influence of the

Poisson effect is to reduce the magnitude of fracture closure on the fracture perpendicular to the applied strain, as matrix is effectively "stiffened", and to induce closure on fractures orthogonal to this direction. When $\nu \to 0$, $H \to 0$, the off-diagonal terms are null, and the principal terms are identical to those used in the body of the paper. Similarly when $R_m \to 0$, representative of very soft joints, $H \to 0$ and the Poisson effect is again null, since negligible matrix strains are developed in the compression of the matrix–fracture system. When $R_m = 1$, the rock mass deforms as intact material and lateral stresses are developed in the ratio $H \to \nu/(1-\nu)$, defining the corresponding reduction of apertures on fractures oriented parallel to the direction of strain or load application. Relations of added complexity may be developed to represent different inital apertures, spacing and stiffness characteristics of the component fractures, as needed.

References

[1] Pusch R. Alteration of the hydraulic conductivity of rock by tunnel excavation. Int J Rock Mech Min Sci & Geomech Abstr 1989;26(1):79–83.

[2] Smelser RE, Richmond O, Schwerer FC. Iteraction of compaction near mine openings and drainage of pore fluids from coal seams. Int J Rock Mech Min Sci & Geomech Abstr 1984;21:13–20.

[3] Skoczylas F, Henry JP. A study of the intrinsic permeability of granite to gas. Int J Rock Mech Min Sci & Geomech Abstr 1995;32(2):171–9.

[4] Zhang L, Franklin JA. Prediction of water flow into rock tunnels: an analytical solution assuming an hydraulic conductivity gradient. Int J Rock Mech Min Sci & Geomech Abstr 1993;30(1):37–46.

[5] Wei ZQ, Egger P, Descoeudres F. Permeability predictions for jointed rock masses. Int J Rock Mech Min Sci & Geomech Abstr 1995;32(3):251–61.

[6] Jakubick AT, Franz T. Vacuum testing of the permeability of the excavation damaged zone. Rock Mech Rock Engng 1993;26(2):165–82.

[7] Patton SB, Fan H, Novak T, Johnson PW, Sanford RL, Simulator for degasification, methane emission prediction and mine ventilation, Mining Engineering 1994;341–45 [April].

[8] Valliappan S, Zhang W. Numerical modeling of methane gas migration in dry coal seams. Int J for Numerical and Analytical Methods in Geomechanics 1996;20:571–93.

[9] Neate CJ, Whittaker BJ. Influence of proximity of longwall mining on strata permeability and ground water. In: Proceedings of US 22th Symposium on Rock Mechanics. The University of Texas at Austin, 1979. p. 217–24.

[10] Booth CJ. Hydrogeologic impacts of underground (longwall) mining in the illinois basin. In: Peng SS, editor. Proc. of Third Workshop on Surface Subsidence due to Underground Mining. Morgantown: Department of Mining Engineering, West Virginia University, 1992. p. 222–7.

[11] Walker JS. Case study of the effects of longwall mining induced subsidence on shallow ground water sources in the Northern Appalachian Coalfield. RI9198, Bureau of Mines, United States Department of the Interior, 1988.

[12] Roosendaal Van DJ, et al. Overburden deformation and hydrological changes due to longwall mine subsidence in illinois. In: Chugh YP, editor. Proceedings of 3rd Conference on Ground Control Problems in the Illinois Coal Basin, Mt. Vernon, IL, 1990. p. 73–82.

[13] Matetic RJ, Trevits MA, Swinehart T. A case study of longwall mining and near-surface hydrological response. In: Proceedings of American Mining Congress-Coal Convention, Pittsburgh, PA, 1991.

[14] Matetic RJ, Trevits M. Longwall mining and its effects on ground water quantity and quality at a mine site in the northern applachian coal field. In: Proceedings of FOCUS Conference on Eastern Regional Ground Water Issues, 1992 October 13–15.

[15] Matetic RJ. An assessment of longwall mining-induced changes in the local ground water system. In: Proceedings of FOCUS Conference on Eastern Regional Ground Water Issues, 1993 September 27–29.

[16] Matetic RJ, Liu J, Elsworth D. Modeling the effects of longwall mining on the ground water system. In: Daemen JJK, Schiltz RA, editors. Proceedings of the 35th U.S. Symposium on Rock Mechanics, 1995. p. 639–44.

[17] Kelsall PC, Case JB, Chabannes CR. Evaluation of excavation-induced changes in rock permeability. Int J Rock Mech Min Sci & Geomech Abstr 1984;21(3):123–35.

[18] Bai M, Elsworth D. Transient poroelastic response of equivalent porous media over a mining panel. Engineering Geology 1993;35:49–64.

[19] Bai M, Elsworth D. Dual-porosity poroelastic approach to behavior of porous media over a mining panel. Trans Inst Min and Metall 1993;102:A114–A124.

[20] Bai M, Elsworth D. Modeling of subsidence and stress-dependent hydraulic conductivity for intact rock and fractured porous media. Rock Mech and Rock Engng 1994;27(4):209–34.

[21] Ouyang Z, Elsworth D. Evaluation of groundwater flow into mined panels. Int J Rock Mech Min Sci & Geomech Abstr 1993;30(2):71–9.

[22] Liu J, Elsworth D. Three-dimensional effects of hydraulic conductivity enhancement and desaturation around mined panels. Int J Rock Mech Min Sci 1997;34(8):1139–52.

[23] Bieniawski ZT. Determinating rock mass deformability: experience from case histories. Int J Rock Mech and Min Sci 1978;15:237–48.

[24] Bieniawski ZT. The geomechanics classification in rock engineering applications. In: Proceedings of the 4th International Congress on Rock Mechanics, Montreaux, 1979. p. 41–8.

[25] Sen Z. Theoretical RQD-porosity-conductivity-aperture charts. Int J Rock Mech Min Sci & Geomech Abstr 1997;33(2):173–7.

[26] Nicholson GA, Bieniawski ZT. A nonlinear deformation modulus based on rock mass classification. Int J of Mining and Geological Engineering 1990;8:181–202.

[27] Mohammad N, Reddish DJ, Stace LR. The relation between in-situ and laboratory rock properties used in numerical modeling. Int J Rock Mech Min Sci & Geomech Abstr 1997;34(2):289–97.

[28] Castillo E. Mathematical model for two-dimensional percolation through fissured rock. In: Proceedings of International Symposium on Percolation through Fissured Rock, Stuttgart, Germany, 1972. p. T1–D1-7.

[29] Panda BB, Kulatilake PHSW. Study of the effect of joint geometry parameters on the permeability of jointed rock. In: Daemen JK, Schiltz RA, editors. Proceedings of 35th U. S. Symposium on Rock Mechanics, Reno, University of Nevada, 1995. p. 273–8.

[30] Snow DT. Anisotropic permeability of fractured media. Water Resour Res 1969;5(6):1273–89.

[31] Witherspoon PA, Wang YSY, Gale JE. Validity of cubic law for fluid flow in a deformed fracture. Water Resources Research 1980;16:1016–24.

[32] Priest SD, Hudson J. Discontinuity spacing in rock. Int J Rock Mech Min Sci & Geomech Abstr 1976;13:135–48.

[33] Charlez PA. Rock Mechanics: Theoretical Fundamentals. Editions Technip, 1991.